

Principal Sub-manifolds

September 30, 2017

Zhigang Yao
Department of Statistics and Applied Probability
21 Lower Kent Ridge Road
National University of Singapore, Singapore 117546
email: zhigang.yao@nus.edu.sg

Tung Pham
School of Mathematics and Statistics
University of Melbourne
Victoria 3010 Australia
email: pham.t@unimelb.edu.au

Abstract

We revisit the problem of finding principal components to the multivariate datasets, that lie on an embedded nonlinear Riemannian manifold within the higher-dimensional space. Our aim is to extend the geometric interpretation of PCA, while being able to capture the non-geodesic form of variation in the data. We introduce the concept of a principal sub-manifold, a manifold passing through the center of the data, and at any point on the manifold, it moves in the direction of the highest curvature in the space spanned by eigenvectors of the local tangent space PCA. Compared to the recent work in the case where the sub-manifold is of dimension one [18]—essentially a curve lying on the manifold attempting to capture the one-dimensional variation—the current setting is much more general. The principal sub-manifold is therefore an extension of the principal flow, accommodating to capture the higher dimensional variation in the data. We show the principal sub-manifold yields the ball spanned by the usual principal components in Euclidean space. By means of examples, we illustrate how to find, use and interpret principal sub-manifold with an extension of using it in shape analysis.

Keywords: manifold, principal component analysis, tangent space, dimension reduction, shape analysis

1 Introduction

Not all data are Euclidean or linear. Manifold data arises in the sense that the sample space of data is fundamentally nonlinear. Among them, there are data that can be seen as lying on spheres dating back as early as [2] in directional statistics, or more generally, as lying on Riemannian manifolds in shape deformation. The latter in particular has posed

an interesting question to study the linkage between the data space, e.g., configurations of landmarks representing a population, and the induced curved shape space. The aim is to make useful statistical inference with respect to the underlying manifold space suggested by the data. To accomplish this goal, a basic step is to transfer the usual coordinate system of the data to a new one indicating its position on the manifold. This can be done either by transforming it to a so-called “known manifold” [15] or by learning an “unknown manifold.” In this paper, we will mainly focus on the known manifold scenario. This kind of problem becomes increasingly important, as many procedures in medical imaging [23, 5] and computer vision produce data [21, 19] in such forms. The differences are that although one can view each observation such as an image as a point in a high-dimensional space, it is more likely to represent a collection of such images using a lower dimensional nonlinear manifold. In a real application, working with the manifold space can help reduce the uncertainty, as it provides more reasonable distance metrics. However, the methodology built directly upon manifold space is still underdeveloped. The primary reason is that conventional statistical methodology based on vector space is not so adaptive when it comes to manifold space. The simplest case is that the notation of sample mean on manifold does not guarantee the existence and uniqueness anymore [13, 14]. To quantify statistical variation on more complex features such as curves and surface, a strategy of developing statistical tools in parallel with their Euclidean-counterpart is significantly relevant.

There have been a number of studies on manifold space over the past decades, most of which try to find the center and the main modes of variation in the data, provided with a curved metric. Roughly speaking, one first expects to find reasonable means of the data (called Fréchet means) and standard deviations, and then find a certain sub-manifold almost explaining the variability of data. Though we have witnessed an increasing effort in developing statistical approaches based on nonlinear manifolds, seemingly from various perspectives, the major effort has been focused on extending the principal component analysis (PCA) to a manifold version. Equipped with Riemannian metrics on shape space, principal geodesics [4, 9, 8, 16, 10, 22, 20] is a manifold version of PCA by replacing the straight lines in Euclidean space with its geodesic analogue on manifolds. Geodesic fitting approaches try to define smooth curves directly in shape space, with reference to the *preshape* space. Using more general spline functions of a certain type on manifolds [12] and [17] developing smooth curves by unrolling and unwrapping the shape space primarily involves transportation of the target curve between the manifold and the tangent space at the starting point—usually sequentially indexed. By finding a sequence of nested linear sub-manifolds (essentially spheres, [10]) with decreasing dimensionality, the principal nested spheres decompose the sample space locally near the mean by sequentially “fitting” within each dimension such that these linear subspaces maximize the variance of the projected data [4]. Tangent space PCA [3] attempts to project the manifold data by simply lifting them to the relevant tangent space, and approximate the data distribution locally at the lifting point on the manifold with the induced Euclidean space. The use of tangent space on one hand makes manifolds much easier to work with, as it allows for tractable statistics; on the other hand, this generalization of PCA is conservative in the sense that the results are more guaranteed when the data clouds are concentrated. By retaining the classical PCA interpretation at each point of the curve, the principal flow [18] is a recently developed approach. Defined upon the manifold, the flow attempts to follow the main direction of the data cloud locally, nevertheless being able to accommodate the “curve fitting” characteristic on the manifold, and therefore admits a global property.

We consider generalizations for principal flow. The idea is to generalize the flow to a

surface or more generally a sub-manifold. The heuristic is the following: if one expects the majority of a data cloud to follow roughly a sub-manifold with an intrinsic dimension more than one, then it is crucial to describe the space of all possible sub-manifolds. In finding such a sub-manifold, we start from the center of the data cloud or any other point of symmetry on the manifold, just like the principal flow; but unlike the principal flow that moves along the maximum direction of variation of the data, we let the sub-manifold expand in all directions simultaneously. In principle, the sub-manifold is not supposed to move equally in any direction. Rather, it is expected to move around guided by the eigenvectors of the local covariance matrix. To form such a sub-manifold with an appropriate expansion, the curvature plays an essential role.

However, identifying a potentially better sub-manifold out of all the possible ones can be non-trivial. It is essentially an optimization problem that consists of comparing one surface with another, subjected to some smooth conditions. The same problem has appeared in finding the principal flow. With this being said, parameterizing curves is much easier than parameterizing surfaces as the latter requires integration along the surface. We introduce two definitions of the principal sub-manifold; the first definition is a conceptual one that does not rely on the actual parameterization of the surface, and the second definition involves a specific parameterization of the surface, and therefore is a concrete one. Although both definitions seem sound, the algorithm of finding the principal sub-manifold is given based on the second definition.

We formally define the principal sub-manifold (Section 2.4) as a sub-manifold in which at any point of the sub-manifold, the tangent space of the sub-manifold attempts to be close to that of the data manifold; intuitively, this definition is an analogue to the definition of the principal flow. We show that in case of flat space, the principal sub-manifold reduces to the ball spanned by the usual principal components, in which the dimension of the sub-manifold corresponds to the number of principal components. Theorem 1 is proved in Appendix. The principal sub-manifold also provides a complementary notation to that of a principal surface by [6], as a self-consistent surface defined in Euclidean space.

The remaining part of the paper is organized as follows. We start with an overview of the principal flow with some necessary background on Riemannian geometry and statistical shape analysis (Section 2.1-2.3). In Section 3, we first investigate an algorithm for determining the principal sub-manifold; then we describe the representation of the principal sub-manifold, with a special example of visualizing a two-dimensional sub-manifold for data in $S^3 \subset \mathbb{R}^4$. Section 4 contains examples; we illustrate by means of simulated examples and the analysis of leaf growth data and handwritten data that the principal sub-manifold is capable of representing more general aspects of data variation compared to the principal flow. We end this paper with a discussion.

2 Principal Sub-manifolds

2.1 Preliminaries

Suppose that $\{x_1, \dots, x_n\}$ are n data points on a complete Riemannian manifold (\mathcal{M}, g) of dimension m , isometrically embedded in the linear space \mathbb{R}^d , where $m < d$.

Throughout the paper, we assume that there always exists a differentiable function $F : \mathbb{R}^d \rightarrow \mathbb{R}^m$ such that

$$\mathcal{M} := \left\{ x \in \mathbb{R}^d : F(x) = 0 \right\}.$$

For each $x \in \mathcal{M}$, the tangent space at x will be denoted by $T_x\mathcal{M}$. Then $T_x\mathcal{M}$ is characterized by the equation

$$T_x\mathcal{M} = \left\{ z : DFz = 0, z \in \mathbb{R}^d \right\}.$$

Thus, $T_x\mathcal{M}$ is in fact a *vector space*, the set of all tangent vectors to \mathcal{M} at x , which essentially provides a local vector space approximation of the manifold \mathcal{M} . This is by analogue the derivative of a real-valued function that provides a local approximation of the function. Let g be a smooth family of inner product associated with the manifold \mathcal{M} :

$$g_x : T_x\mathcal{M} \times T_x\mathcal{M} \rightarrow \mathbb{R}$$

Then for any $v \in T_x\mathcal{M}$, the norm of v is defined by

$$\|v\| = g_x(v, v).$$

Definition 2.1 A curve, $\gamma : [0, \delta] \rightarrow \mathcal{M}$ is a geodesic if and only if $\dot{\gamma}(t)$ is parallel along γ , that is, the acceleration vector

$$\frac{d(\dot{\gamma})}{dt} = 0,$$

where δ is sufficiently small such that the curve is well-defined. The definition means that $\frac{d(\dot{\gamma})}{dt}$ is normal to $T_{\gamma(t)}\mathcal{M}$ at any time t .

By equipping the manifold with the tangent space, we define mappings back and forth between $T_x\mathcal{M}$ and \mathcal{M} . There are two kinds of mappings of interest: 1) the exponential map being well defined in terms of geodesics, is the map,

$$\exp_x : T_x\mathcal{M} \rightarrow \mathcal{M} \tag{2.1}$$

by $\exp_x(v) = \gamma(\|v\|)$ with γ is a geodesic starting from $\gamma(0) = x$ with initial velocity $\dot{\gamma}(0) = v/\|v\|$ and $\|v\| \leq \delta$, and 2) the logarithm map (the inverse of exponential map), is locally defined at least in the neighborhood of x ,

$$\log_x : \mathcal{M} \rightarrow T_x\mathcal{M}. \tag{2.2}$$

Here, the **exp** and **log** are defined on a local neighborhood of 0 and x such that they are all well-defined away from the locus of x on \mathcal{M} .

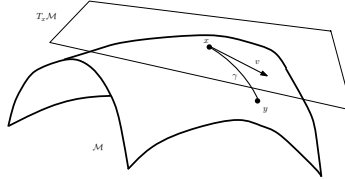


Figure 1: The vector v on the tangent subspace $T_x\mathcal{M}$ at x . The endpoint of vector v is the image of $y = \exp_x(v)$ under the mapping defined in (2.2).

Let $x, y \in \mathcal{M}$. Denote all (piecewise) smooth curves $\gamma(t) : [0, 1] \rightarrow \mathcal{M}$ with endpoints such that $\gamma(0) = x$ and $\gamma(1) = y$. The *geodesic distance* from x to y is defined as

$$d_{\mathcal{M}}(x, y) = \inf \ell(\gamma) \quad (2.3)$$

where $\ell(\gamma) = \int_{[0,1]} \|\dot{\gamma}(t)\| dt = \int_{[0,1]} g_{\gamma(t)}(\dot{\gamma}(t), \dot{\gamma}(t))^{\frac{1}{2}} dt$. Minimizing (2.3) yields geodesics as in Definition 2.1, the shortest distance between two points x and y in \mathcal{M} .

Definition 2.2 *The Fréchet mean, $\bar{x} \in M$, for a sample of data points $\{x_1, \dots, x_n\} \in \mathcal{M}$ is a minimizer of the Fréchet variance, if the minimizer is unique:*

$$\bar{x} = \operatorname{argmin}_{x \in \mathcal{M}} \frac{1}{n} \sum_{i=1}^n d_{\mathcal{M}}^2(x, x_i).$$

2.2 Embedding of shape space for landmarks

From shape analysis view point, landmark coordinates retain the geometry of a certain point configuration. The landmarks are observations, which are usually positions or correspondences on an object in an appropriate coordinate axes. Consider a suitable ordered set of k landmarks of an object, namely a k -ad (where $k \geq 2$), with each landmark lying in $\mathbb{R}^{d'}$. That is,

$$z = \left\{ z^j \in \mathbb{R}^{d'} : 1 \leq j \leq k \right\},$$

One would like to know how a certain shape of an object out of a collection of several z 's differs from the other. As an object's shape should not change under translation, scaling or rotation, two objects with the same shape should line up exactly. Here, we briefly mention a shape matching representation called Kendall shape space ($\Sigma_{d'}^k$), which is invariant under translation, scaling, and rotation. The following steps lead to transforming any k -ad, z , to a point on the unit sphere:

Translation: remove the effects of translation by $z^* = z - \bar{z}$, where $\bar{z} = \frac{1}{k} \sum_{j=1}^k z^j$

Normalization: remove the effect of scaling by $z_{\text{pre}} = \frac{z^*}{\|z^*\|}$

Rotation: $[z] = R(\theta)z_{\text{pre}} = e^{i\theta}z_{\text{pre}}$, where $-\pi < \theta \leq \pi$.

Remarks: It's worthwhile to note that, although Kendall shape space can be valid for $d' \geq 2$, the rotation step is in fact only valid when $d' = 2$. Of interest, we mainly consider translation and normalization step. We restrict $d' = 2$ for completion: the translated z^* lies in the hyperplane of \mathbb{R}^{2k-2} ; after translation and normalization, z_{pre} is called the *preshape* of z . The space of z_{pre} is identified as the unit sphere $S^{2k-3} \subset \mathbb{R}^{2k-2}$. Here “-2” comes from losing 2 degrees of freedom in the translation step, and “3” comes from the definition of unit sphere

$$S^k = \left\{ v \in \mathbb{R}^{k+1} : \|v\| = 1 \right\}. \quad (2.4)$$

The $[z]$ is the *shape* of z given by the *orbit* of the preshape z_{pre} under rotation. The Σ_2^k is a quotient space of S^{2k-3} with dimension $2k - 4$. This shape space is the equivalent classes of all such k -ads after removing the effects of translation, scaling and rotation.

2.3 Principal flows

Before introducing the principal sub-manifold, we recall the concept of the principal flow, which has been proposed to capture the non-geodesic variation of a given set of data points $\{x_1, \dots, x_n\}$ lying on a manifold \mathcal{M} .

Here, we briefly review the flow using the sub-manifold representation (see [18] for a full treatment and its original definition). It is chosen as a matter of convenience in later derivations and can be thought of as drawing a connection to the principal sub-manifold. As any flow on \mathcal{M} is a one dimensional sub-manifold of \mathcal{M} , we can parameterize the one dimensional sub-manifold explicitly using a unit speed curve as follows

$$\text{SubM}(A, 1, v, \mathcal{M}) = \left\{ \gamma : [0, r] \rightarrow \mathcal{M}, \gamma \in C^2(\mathcal{M}), \gamma(s) \neq \gamma(s') \text{ for } s \neq s', \right. \\ \left. \gamma(0) = A, \dot{\gamma}(0) = v, \ell(\gamma[0, t]) = t \text{ for all } 0 \leq t \leq r \leq 1 \right\}. \quad (2.5)$$

where $\gamma(0) = A$ and $\dot{\gamma}(0) = v$ are initial conditions for γ and $\ell(\gamma)$ is the length of γ . The starting point A can be chosen as the Fréchet mean \bar{x} or any other point of interest. This says that $\text{SubM}(A, 1, v, \mathcal{M})$ contains all smooth curves with a given initial speed and a starting point, as well as their length being all less than 1.

To find a curve from the set in (2.5), the principal flow is defined as a solution that involves two curves γ^+ and γ^- to the following variational problem

$$\gamma^+ = \arg \sup_{\gamma \in \text{SubM}(A, 1, v_1, \mathcal{M})} \int_0^{\ell(\gamma)} \langle \dot{\gamma}(t), e_1(\gamma(t)) \rangle dt \quad (2.6)$$

$$\gamma^- = \arg \inf_{\gamma \in \text{SubM}(A, 1, v_2, \mathcal{M})} \int_0^{\ell(\gamma)} \langle \dot{\gamma}(t), e_1(\gamma(t)) \rangle dt \quad (2.7)$$

where $v_1 = e_1(\gamma(t))$, $v_2 = -v_1$, $e_1(\gamma(t))$ is the first eigenvector of the covariance matrix $\Sigma_{\gamma(t)}$ at $\gamma(t)$. The integral for γ^- is negative, which explains why the infimum appears in its definition. At each point of γ , $\dot{\gamma}(t)$, is maximally compatible to the eigenvector of local PCA at the same point. Often, the local covariance matrix at scale h is used

$$\Sigma_{h, \gamma(t)} = \frac{1}{\sum_i \kappa_h(x_i, \gamma(t))} \sum_{i=1}^n \mathbf{log}_{\gamma(t)}(x_i) \otimes \mathbf{log}_{\gamma(t)}(x_i) \kappa_h(x_i, \gamma(t)) \quad (2.8)$$

where $y \otimes y := yy^T$ and $\kappa_h(x, \gamma(t)) = K(h^{-1}d_{\mathcal{M}}(x, \gamma(t)))$ with a smooth non-increasing kernel K on $[0, \infty]$. We remark here that all the above definitions are under the assumption that the first and second eigenvalues of $\Sigma_{h, \gamma(t)}$ are distinct.

The viewpoint of the [18] is two-fold: to differentiate from principal geodesic curves, principal flow is not necessarily a geodesic on the manifold, which gives an opportunity to capture non-geodesic variation from the manifold data; to differentiate from other curve-fitting approaches, principal flows are data dependent and quite flexible in trading-off the local PCA and the curve fitting characteristic.

We now adopt their view point, and partial adopting their notation. Our question becomes: can we capture more nonlinear variation by extending the principal flow to a higher dimensional manifold. Such questions have been discussed (for other assumption of the embedding data space) under the names of *principal curves* or *principal surfaces*

[6]. Note that the principal surfaces are the extension of the principal curves to higher dimensions in Euclidean space, restricted to a two-dimensional scenario. The following work is connected to both principal flow and the principal surfaces, but the setting it entails are more general. In our work, we use principal sub-manifold, to denote the multi-dimensional manifold aforementioned. We remark that the principal sub-manifold is only generic for the work done here, admittedly being less than encyclopedic about other scholarly contributions in differential geometry and manifold learning literature [24].

2.4 Principal sub-manifolds

As before, denote $\{x_1, \dots, x_n\}$ to be the data points on \mathcal{M} . We will give the definition of a multi-dimensional manifold, starting from a point of interest x on \mathcal{M} . The manifold is denoted as \mathcal{N} , which is a sub-manifold of \mathcal{M} .

For any point x in \mathcal{M} , following (2.8), define the local tangent covariance matrix on \mathcal{M}

$$\Sigma_{h,x,\mathcal{M}} = \frac{1}{\sum_i \kappa_h(x_i, x)} \sum_{i=1}^n \log_{x,\mathcal{M}}(x_i) \otimes \log_{x,\mathcal{M}}(x_i) \kappa_h(x_i, x). \quad (2.9)$$

To fix notation, from now on, we will only use $\Sigma_{x,\mathcal{M}}$ by dropping the subscript h . Let $\{\lambda_1(x, \mathcal{M}), \dots, \lambda_k(x, \mathcal{M})\}$ and $\{e_1(x, \mathcal{M}), \dots, e_k(x, \mathcal{M})\}$ be the first k eigenvalues and eigenvectors of $\Sigma_{x,\mathcal{M}}$. Denote $H_k(x, \mathcal{M})$ the linear subspace spanned by $\{e_1(x, \mathcal{M}), \dots, e_k(x, \mathcal{M})\}$, and $H_k(x, \mathcal{N})$ the tangent space of \mathcal{N} at x .

The key implication of finding the sub-manifold is to re-consider the relation of eigenvector and tangent vector as in the case of principal flow, which may mean, from a geometrical viewpoint, that sub-manifold corresponds to extending the linear subspace $H_k(x, \mathcal{M})$ and the tangent space $H_k(x, \mathcal{N})$ naturally. Note that in finding a principal flow, we have used that fact that its curves are well parameterized and the integral along the curve is invariant under different parameterizations; the latter plays a key role in determining principal flow, but is unfortunately an obstacle for general sub-manifolds with dimensions more than one. Thus, for the higher dimensional sub-manifold, we define the sub-manifold locally.

For any point x belonging to the sub-manifold \mathcal{N} , define

$$\mathbf{B}(x, \mathcal{N}, \epsilon) = \left\{ y \in \mathcal{N} : d_{\mathcal{N}}(x, y) \leq \epsilon \right\}.$$

where $d_{\mathcal{N}}(x, y)$ is the distance of x and y on \mathcal{N} . For any positive integer number $k < m$, and any point $x \in \mathcal{M}$, let $\text{SubM}(x, \epsilon, k, \mathcal{M})$ be the set of all k -dimensional sub-manifolds, not intersecting themselves, of $\mathbf{B}(x, \mathcal{M}, \epsilon)$.

For a given k , the main idea of our principal sub-manifold is that at each point B of the sub-manifold \mathcal{N} , the sub-manifold should be able to explain the manifold variation as much as possible. To measure the degree of such variation for a potential sub-manifold, one way is to use the angle α_B , which is the Asimov distance between the two linear subspaces, $H_k(B, \mathcal{M})$ and $H_k(B, \mathcal{N})$. Geometrically, this is somehow an analogue to the angle between the tangent vector and eigenvector in the principal flow. Here, on each point B , the tangent space $H_k(B, \mathcal{N})$ bends towards the linear subspace $H_k(B, \mathcal{M})$ at the same point. Theoretically, if $\alpha_B = 0$ for every B , then $H_k(B, \mathcal{M}) = H_k(B, \mathcal{N})$. For general cases, one would hope α_B is as small as possible. Therefore, it seems naturally that one would integrate the sub-manifold by

$$\arg \sup_{\mathcal{N} \in \text{SubM}(A, \epsilon, k, \mathcal{M})} \int_{B \in \mathcal{N}} \left(\cos(\alpha_B) \times \sum_{j=1}^k \lambda_j(B, \mathcal{M}) \right) d\mu_{\mathcal{N}}, \quad (2.10)$$

where $\mu_{\mathcal{N}}$ is the Riemannian (volumn) measure on \mathcal{N} .

Despite the quite natural expectation that the above extension to sub-manifold case ought to be practically feasible, its realization is not so direct. As we can see, the principal sub-manifold in (2.10) is not attached to any specific parameterization of the sub-manifold \mathcal{N} . However, working with this definition requires integration without knowing its parameterization, which can be quite challenging. Recall that in (2.6), one can reparameterize the curve so that its velocity is a unit vector. This allows comparing curves to curves by their length. For sub-manifold in (2.10), where the integral would be taken over a multi-dimensional sub-manifold, having a unit-speed parameterization is perhaps unexpectedly feasible. In words, unlike the principal flow, that is invariant under different reparameterization, the sub-manifold does not enjoy this property.

To have tractable sub-manifold, we consider two ways of approximating the sub-manifold. We pick the following two steps:

- (1) mapping \mathcal{N} to an image $L(\mathcal{N}, \epsilon)$ (essentially an ϵ -ball) onto the tangent space, and
- (2) parameterizing the sub-manifold under the image of by polar coordinates.

Here, we choose $L(\mathcal{N}, \epsilon) := \log_A(\mathcal{N}_\epsilon) = \left\{ \log_A(B) : B \in \mathbf{B}(A, \mathcal{N}, \epsilon) \right\}$; that is, $L(\mathcal{N}, \epsilon)$ is the image of the sub-manifold \mathcal{N}_ϵ at A under the logarithm map. For a better presentation, we will ignore the subscript ϵ in $\log_A(\mathcal{N}_\epsilon)$ and use $\log_A(\mathcal{N})$ whenever there is no confusion.

In line with the two steps, we gradually advance the definition of the principal sub-manifold and arrive at two definitions. The two definitions which are inter-connected with each other are summarized as Definition 2.3 and Definition 2.4. The connection between the two definitions will be further illustrated in Figure 2.

Definition 2.3 *Assume that the first $k + 1$ eigenvalues of $\Sigma_{B, \mathcal{M}}$ are distinct, with any point $B \in \mathcal{N}$ and $\mathcal{N} \in \text{SubM}(A, \epsilon, k, \mathcal{M})$. Denote $\lambda_1(B, \mathcal{M}), \dots, \lambda_k(B, \mathcal{M})$ the first k eigenvalues of $\Sigma_{B, \mathcal{M}}$. The k -dimensional principal sub-manifold is defined as follows*

$$\arg \sup_{\mathcal{N} \in \text{SubM}(A, \epsilon, k, \mathcal{M})} \int_{\log_A(B) \in \log_A(\mathcal{N})} \left(\cos(\alpha_B) \times \sum_{j=1}^k \lambda_j(B, \mathcal{M}) \right) d\mu_k(\log_A(\mathcal{N})),$$

where μ_k is the Lebesgue measure on the k -dimensional space.

From Definition 2.3 naturally relaxes the ideal sub-manifold by replacing the integral with that being restricted on the image of the sub-manifold; that is, $d\mu_{\mathcal{N}}$ in (2.10) is replaced by $d\mu_k$. From Definition 2.3 (Figure 2(b)), we see that when $k = 1$, the sub-manifold \mathcal{N} is a curve, and the tangent plane $T_B \mathcal{N}$ at B reduces to the tangent vector v_B of the curve \mathcal{N} at point B . In this case, it is not difficult to see that $H_1(B, \mathcal{N})$ is the first eigenvector at B of the covariance matrix $\Sigma_{h, B, \mathcal{M}}$, and hence the measure of B on \mathcal{N} , $\mu_{\mathcal{N}}(B)$, becomes the length of the curve \mathcal{N} (Figure 2(a)). This is equivalent to the definition of principal flow in Definition 2.6. Therefore, the principal sub-manifold is indeed an extension of the principal flow to the higher dimensional scenario, where $k \geq 2$.

In Theorem 1, we show that principal sub-manifold (under Definition 2.3) reduce to the ball spanned by usual principal components, in the context of Euclidean spaces. The proof of the theorem can be found in the Appendix.

THEOREM 1 Assume that $\mathcal{M} = \mathbb{R}^d$ and the first $k + 1$ eigenvalues of $\Sigma_{B,\mathcal{M}}$ are distinct, with any point $B \in \mathcal{N}$ and $\mathcal{N} \in \text{SubM}(A, \epsilon, k, \mathcal{M})$. Denote $\lambda_1(B, \mathcal{M}), \dots, \lambda_k(B, \mathcal{M})$ the first k eigenvalues of $\Sigma_{B,\mathcal{M}}$. Then

$$\begin{aligned} \arg \sup_{\mathcal{N} \in \text{SubM}(A, \epsilon, k, \mathcal{M})} & \int_{\log_A(B) \in \log_A(\mathcal{N})} \left(\cos(\alpha_B) \times \sum_{j=1}^k \lambda_j(B, \mathcal{M}) \right) d\mu_k(\log_A(\mathcal{N})) \\ &= \text{The ball of radius } \epsilon \text{ centered at } A \text{ in the linear space spanned by} \\ &\quad \{e_1(A, \mathcal{M}), e_2(A, \mathcal{M}), \dots, e_k(A, \mathcal{M})\}, \end{aligned}$$

where $e_1(A, \mathcal{M}), e_2(A, \mathcal{M}), \dots, e_k(A, \mathcal{M})$ are the first k eigenvectors of $\Sigma_{A,\mathcal{M}}$.

Although Definition 2.3 well relates to the principal flow, it remains abstract. To realize the Definition 2.3, the image $L(\mathcal{N}, \epsilon)$ should be further parameterized, so that integration is applicable. In words: since $L(\mathcal{N}, \epsilon)$ lies in an ϵ -ball ($\mathcal{B}^k(\epsilon)$), for any point $D \in L(\mathcal{N}, \epsilon)$, there exists a unique point B such that $B = \exp_A(D)$ lies in \mathcal{N} . It makes sense that we parameterize $L(\mathcal{N}, \epsilon)$ using polar coordinates. For any point $B \in \mathcal{N}$, let v_B be the tangent vector field of a geodesic curve on the sub-manifold \mathcal{N} from A to B , denote α'_B to be the angle between v_B and linear subspace $H_k(B, \mathcal{M})$ (Figure 2(c)). Here α'_B is chosen to replace α_B . Although α'_B does not necessarily equal α_B for every B , this modification not only measures how \mathcal{N} differs from \mathcal{M} at B , but also provides a convenient construction of a surface of maximal ‘‘cumulative variation.’’ Arguably, it appears to be more natural to work with this definition, as the integral can be approximated based on the polar coordinates.

Definition 2.4 Assume that the first $k + 1$ eigenvalues of $\Sigma_{B,\mathcal{M}}$ are distinct, with any $B \in \mathcal{N}$ and $\mathcal{N} \in \text{SubM}(A, \epsilon, k, \mathcal{M})$. Denote $\lambda_1(B, \mathcal{M}), \dots, \lambda_k(B, \mathcal{M})$ the first k eigenvectors of $\Sigma_{B,\mathcal{M}}$. The k -dimensional principal sub-manifold is defined as follow

$$\arg \sup_{\mathcal{N} \in \text{SubM}(A, \epsilon, k, \mathcal{M})} \int_{\log_A(B) \in \log_A(\mathcal{N})} \left(\cos(\alpha'_B) \times \sum_{j=1}^k \lambda_j(B, \mathcal{M}) \right) d\mu_k(\log_A(\mathcal{N})), \quad (2.11)$$

where μ_k is the Lebesgue measure on the k -dimensional space.

Remark Definition 2.4 is almost identical to Definition 2.3. A similar theorem for Definition 2.4 could be easily stated and proved; hence we omit them.

We conclude this session with a remark on the interpretation of Theorem 1. The result of Theorem 1 shows that, in a flat space, the principal sub-manifold reduces to a k -dimensional ball in the space spanned by the k eigenvectors of $\Sigma_{A,\mathcal{M}}$ when $h = \infty$. In connection with the principal flow, recall the similar result in principal flow (Proposition 5.1, [18]) where the first order of the principal flow on a flat space has been shown to coincide with the first principal direction with a condition that the locality parameter h of the tangent covariance matrix is chosen to be infinity.

3 Determination of Principal Sub-manifold

3.1 An algorithm for principal sub-manifold

Recall that the principal flow is the solution of an optimization problem in (2.6) or (2.7). To find such a solution, it requires extensive searching for a critical point of a Euler-Lagrange

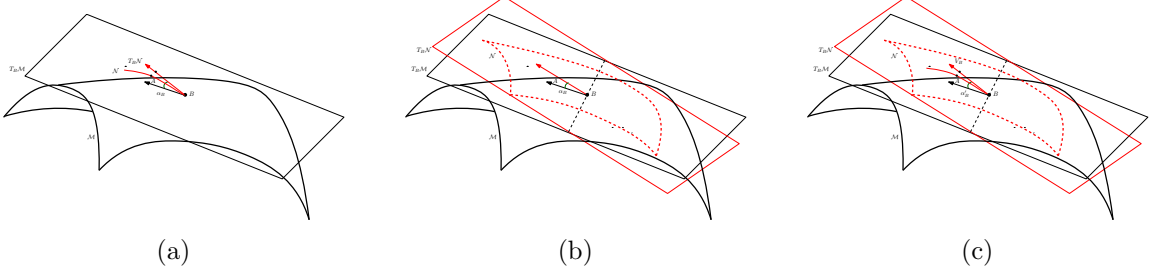


Figure 2: Principal sub-manifolds. (a) Principal flow (α_B is the angle between $T_B \mathcal{N}$ ($k = 1$) and $T_B \mathcal{M}$ ($k = 1$)); (b) Principal sub-manifold (in Definition 2.3, α_B is the angle between $T_B \mathcal{N}$ ($k \geq 2$) and $T_B \mathcal{M}$ ($k \geq 2$)); (c) Principal sub-manifold (in Definition 2.4, α_B is the angle between v_B on $T_B \mathcal{N}$ ($k \geq 2$) and $T_B \mathcal{M}$ ($k \geq 2$))

problem that involves integrating the vector field along the curve. Because it is a one dimensional curve, numerical methods are coincidentally helpful as shown in [18], in that it reduces to a problem of determining the solution of a system of ordinary differential equations (ODEs). As seen in (2.11), when it comes to a sub-manifold from, things turn out to be quite different. Numerically efficient procedures to the corresponding optimization problem for the sub-manifold is unfortunately very limited in our setting. The main reason is that, one needs a much more sophisticated Lagrange formulation to optimize over a chosen sub-manifold with a very different initial condition; whereas in the case of principal flow one only needs a starting point and an initial speed.

At this point, we remark here that there is no fundamental difference of working with a two-dimensional sub-manifold or a higher one under our definitions proposed previously. The only difference lies in the implementation where a sub-manifold with higher dimension would result in higher computational complexity. We will discuss how to determine a two-dimensional principal sub-manifold (e.g., Definition 2.4) as a special case and present an algorithm for the rest of paper. The extension of the algorithm derived here to a higher dimensional sub-manifold is practically feasible.

Now consider $\mathcal{N} \in \text{SubM}(A, \epsilon, k, \mathcal{M})$ where $k = 2$. We will avoid optimizing the integration analytically. Rather, we concern the geometry of Definition 2.4 with its implicitness matched by an approximated solution. To see the connection, note that $\log_A(\mathcal{N})$ is the image of \mathcal{N} at A . As the integration is restricted on the image, it is possible to approximate the ideal optimization of integration by an exploit of the image, as well as the local covariance.

We may divide the image along a number of directions: at every direction on the image, we can approximate the target sub-manifold, or more strictly speaking, a *net* of it, by mimicking the principal flow; each net would be a curve, while not being the exact principal flow, but remaining the property that its tangent vector at each point obeys the local tangent space in an optimal way.

Define l th (i.e., $l \in \mathcal{L} = [1, 2, \dots, L]$) net of the sub-manifold,

$$\mathcal{A}_l = \left(A_{l,0}, A_{l,1}, A_{l,2}, \dots, A_{l,N(l)} \right)^T \quad (3.12)$$

where $N(l)$ is the number of the levels for l th direction. For convenience, we set $L = 180$. Clearly, \mathcal{A}_l contains the points that have been explored along l th direction. This can be interpreted as an effect of cumulative variation. For all directions, we name $A_{l,0} = A$ as the 1st level of all *nets* of the sub-manifold.

In words, the key is to represent \mathcal{N} discretely by a collection of ordered nets, with each one being amount to certain amount of data variation. The nets are expected to grow and expand along all directions. While the principal flow tries to match its tangent vector to the first eigenvector at a certain point in order to attain the maximal, the principal sub-manifold tries to find its best direction that belongs to the plane spanned by the first few eigenvectors. In this sense, those directions that the sub-manifolds would expand provide an extra dimension to build up the target sub-manifold. Many of such nets of sub-manifolds at different levels representing an approximation to the sub-manifold \mathcal{N} at A —in every possible direction of variation—remain to be found.

We call all the nets for all directions a *principal sub-manifold* \mathcal{N} . A complete algorithm (Algorithm 1) can be found in the Appendix. Here, we elaborate the core of the algorithm (see Figure 3): given direction l , we are at the i th level, $A_{l,i}$, there are three steps to go through to find the $(i+1)$ th level, $A_{l,i+1}$

- (1) *Reorientation*: identify the current tangent vector of the curve $A_{l,i}A_{l,i-1}$ and determine the direction for the next move
- (2) *Projection*: expand the points $A_{l,i}$ along the direction $r_{l,i}$ by a step of ϵ' and arrive at point $A_{l,i+1}$
- (3) *Updating*: project the data points x_j 's ($1 \leq j \leq n$) onto the point $A_{l,i+1}$, and recalculate the tangent plane at $A_{l,i+1}$

In step (1), given the current point $A_{l,i}$ and the previous point $A_{l,i-1}$, we obtain the tangent vector of the curve $A_{l,i}A_{l,i-1}$ by

$$v_{l,i} = \log_{A_{l,i}}(A_{l,i-1}).$$

Here the tangent vector $v_{l,i}$ is obtained by backward projection. As the best knowledge we have known about the net at $A_{l,i}$ is $v_{l,i}$. Let $u_{l,i}$ be the direction for the next move. It makes sense to determine $u_{l,i}$ by projecting $v_{l,i}$ to the tangent plane at $A_{l,i}$

$$u_{l,i} = \langle v_{l,i}, e_1(A_{l,i}) \rangle e_1(A_{l,i}) + \langle v_{l,i}, e_2(A_{l,i}) \rangle e_2(A_{l,i})$$

where $e_1(A_{l,i})$ and $e_2(A_{l,i})$ are the first and second eigenvector of $\Sigma_{A_{l,i}, \mathcal{M}}$.

In step (2), we move $A_{l,i}$ on the tangent plane by a step of ϵ' along $r_{l,i}$, where

$$r_{l,i} = -\epsilon' \times \frac{u_{l,i}}{\|u_{l,i}\|},$$

and then map it back to the manifold \mathcal{M}

$$A_{l,i+1} = \exp_{A_{l,i}}(r_{l,i}).$$

Note that $u_{l,i}$ is not of unit length, and the negative sign appears as $u_{l,i}$ is obtained from $v_{l,i}$.

In step (3), the updating of the covariance matrix at $A_{l,i+1}$ is necessary when local data points change significantly, where the covariance matrix $\Sigma_{A_{l,i}, \mathcal{M}}$ can be simply updated by $\Sigma_{A_{l,i+1}, \mathcal{M}}$.

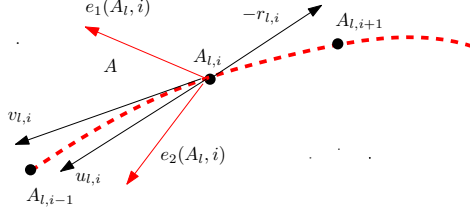


Figure 3: Illustration of the Algorithm. The goal is to determine $A_{l,i+1}$, given the current point $A_{l,i-1}$ and the previous point $A_{l,i}$: $v_{l,i}$ is the tangent vector of the curve $A_{l,i}A_{l,i-1}$, $u_{l,i}$ is the projection of $v_{l,i}$ onto the tangent plane spanned by $e_1(A_{l,i})$ and $e_2(A_{l,i})$. The point $A_{l,i+1}$ is found by mapping a small move ϵ' from $A_{l,i}$ along the direction of $r_{l,i} = -u_{l,i}/\|u_{l,i}\|$.

It is crucial to make sure that the principal sub-manifold always moves forward, which implies that it never moves backward to the points it has already explored. In the meanwhile, a stop condition is also necessary. In accordance with the stopping rule used in [18], we can terminate the process when the *length* of the l th net, i.e.,

$$\ell_{\mathcal{A}_l} = \sum_{i=1}^{N(l)-1} d(A_{l,i}, A_{l,i+1}),$$

exceeds 1. The length of l th net does not necessarily have to be equal. There may exist other stopping rules that one can use. Among them, we should also consider that for all j ,

$$\|\log_{A_{l,i+1}}(x_j)\| > \delta \text{ or } \langle \log_{A_{l,i+1}}(A_{l,i}), \log_{A_{l,i+1}}(x_j) \rangle \geq 0,$$

which implies that either there are not enough data points in the neighborhood or $A_{l,i+1}$ is already outside the convex hull of the x_j 's under the logarithm map.

Remark both ϵ' and δ are pre-defined parameters. We suggest to choose ϵ' favorably with small values, as in this case, small values of ϵ' ensure the stability of the local move on the tangent plane, while the choice of δ depends more on the data dispersion and configuration, which might vary from case to case.

3.2 Visualization of the principal sub-manifold

The principal sub-manifold in general cannot be fully visualized when its dimension exceeds one. Consider a simple case where the data lies in $S^3 \subset \mathbb{R}^4$; the principal sub-manifold is then a subset of S^3 ; that is, it is equivalent to visualizing a two-dimensional manifold in a four-dimensional space. However, a meaningful representation of the sub-manifold is still quite relevant for understanding the manifold variation, at least partially. We propose two ways of visualizing the principal sub-manifold. The first one is to represent the sub-manifold in the principal directions. The second one is to visualize the sub-manifold in the projected manifold space.

- parameterize the sub-manifold in polar coordinates and represent it by the shapes of the principal directions
- project the sub-manifold by multiplying a projection matrix in which the basis is formed by eigenvectors from the covariance matrix at the starting point

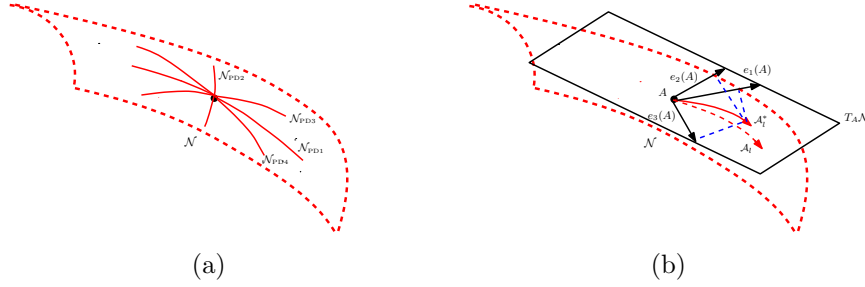


Figure 4: Visualization of a principal sub-manifold. (a) Visualize the sub-manifold by the five principal directions. (b) Visualize the sub-manifold by projecting to the three largest eigenvectors of covariance matrix at A .

Visualization in principal direction: Choose the most varying parts of sub-manifold and visualize the sub-manifold by using these very parts. Recall that the entire sub-manifold can be expressed as follows

$$\mathcal{N} = [\mathcal{A}_1, \mathcal{A}_2, \dots, \mathcal{A}_L]^T.$$

Although we denote \mathcal{N} as a ‘‘matrix’’, the actual length of each row (i.e., $\mathcal{A}_l, 1 \leq l \leq L$) may vary. To visualize the sub-manifold, we select a candidate set $\mathcal{L}_s \subset \mathcal{L}$ and transform the corresponding rows of \mathcal{N} to the corresponding shape coordinates. Thus, the most varying parts of sub-manifold shall be represented by

$$x_{l,i} = f^{-1}(A_{l,i}), \quad \forall l \in \mathcal{L}_s, 1 \leq i \leq N(l),$$

where f is the embedding function. In the case of Kendall shape space, the resultant $x_{l,1}, \dots, x_{l,N(l)}$ is a collection of $N(l)$ k -ads.

Among all l ’s, we call name the following two directions as the *principal directions* of the sub-manifold. Recall polar coordinates on the image $\theta = 2l\pi/L$, where $L = 180$. The first principal direction, denoted as $\mathcal{N}_{\text{PD}1}$, is the curve corresponding to $\theta = \pi$ and $\theta = 2\pi$ in polar coordinates on the image; this is equivalent to l equals 90 and 180 such that

$$\mathcal{N}_{\text{PD}1} = \mathcal{A}_{90} \cup \mathcal{A}_{180}.$$

The second principal direction, denoted as $\mathcal{N}_{\text{PD}2}$, corresponds to the curve with $\theta = \pi/2$ and $\theta = 3\pi/2$ in polar coordinates on the same image; this is equivalent to l equals 45 and 135 such that

$$\mathcal{N}_{\text{PD}2} = \mathcal{A}_{45} \cup \mathcal{A}_{135}.$$

In addition, it is suggested to also include the curves, $\mathcal{N}_{\text{PD}3}$, corresponding to $\theta = \pi/4$ and $\theta = 5\pi/4$ as well as the ones, $\mathcal{N}_{\text{PD}4}$, corresponding to $\theta = 3\pi/4$ and $\theta = 7\pi/4$. Adding two extra directions gives extra details about the sub-manifold.

We remark here that although we have used $\mathcal{N}_{\text{PD}1} - \mathcal{N}_{\text{PD}4}$ as the principal directions, they are by no means the simple extension of the usual principal components or any variants. Figure 4(a) gives an example of such a configuration of shapes. The entire image contains 9 by 9 small shapes. The central figure is the mean shape. Row 5 represents the shapes of $\mathcal{N}_{\text{PD}1}$. Column 5 is the shapes of $\mathcal{N}_{\text{PD}2}$. The main diagonal contains the shapes of $\mathcal{N}_{\text{PD}3}$. The other diagonal contains the shapes $\mathcal{N}_{\text{PD}4}$.

Visualization in projected space: Alternatively, one may wish to represent the sub-manifold using a projected sub-manifold rather than itself. The latter serves as a much

simplified version of the original one and it is more interpretable, provided that the majority of variation of the principal sub-manifold can be explained by a reduced one. Compared to the previous representation, this visualization remains the resolution of the sub-manifold.

To fix representation, we center the \mathcal{N} row-wise by A and obtain the centered sub-manifold

$$\mathcal{N}^* = (\mathcal{N}_{l,i}^*)_{1 \leq l \leq L, 1 \leq i \leq N(l)}$$

where $\mathcal{N}_{l,i}^* = A_{l,i} - A$ where $1 \leq l \leq L, 1 \leq i \leq N(l)$. Clearly, for $i = 1$, $\mathcal{N}_{l,i}^* = \mathbf{0}$. Let the projection matrix for \mathcal{N}^* be

$$\Psi = (\psi_{l,i})_{1 \leq l \leq L, 1 \leq i \leq N(l)},$$

where $\psi_{l,i}$ is the projection matrix for $A_{l,i}$. Usually, we choose $\psi_{l,i} = E_3$ where $E_3 = [e_1(A), e_2(A), e_3(A)]^\top$ of $\Sigma_{A,\mathcal{M}}$. The process is carried out by multiplying \mathcal{N}^* element-wise by the projection Ψ , so that

$$\mathcal{N}^{\text{pro}} = \Psi \odot \mathcal{N}^*$$

where \odot is the element-wise product such that $\mathcal{N}_{l,i}^{\text{pro}} = \psi_{l,i} \mathcal{N}_{l,i}^*$. Figure 4(b) illustrates the main idea: the red dashed arrow starting from A denotes the l th net (or a vector of $(A_{l,1}, \dots, A_{l,N(l)})$) of the principal sub-manifold \mathcal{N} ; the red solid arrow denotes the projected l th net of the principal sub-manifold, \mathcal{A}_l^* . The point A is now regarded as the new origin under the new coordinate system, correspondingly. Moreover, the data points x_j 's are projected in the same way by

$$x_j^* = E_3(x_j - A), \quad 1 \leq j \leq n.$$

In principle, the projected points x_j^* 's are expected to lie closely to the sub-manifold \mathcal{N}^{pro} , provided that the projection matrix has accounted most of the variability.

3.3 A demonstration of the algorithm

To illustrate the principal sub-manifold, we generate a set of data points on $S^3 \subset \mathbb{R}^4$. Readers may refer to supplementary materials for details. The curved surface gives some knowledge about the inherited geometry of the projected sub-manifold. This can be understood by noting that the surface carries an S -pattern that mainly comes from a rough sinusoid of the first triplets. Figure 5 shows the data, the estimated principal sub-manifold, and the super-imposed principal directions. The starting point (in black) is the center of the data points (in red). The two green curves are the first and second principal direction lying on the surface corresponding to the estimated principal sub-manifold (in grey). All of them are projected to the first three eigenvectors of the covariance matrix at the starting point. The surface enables itself to bend wherever the curvature of the manifold changes rapidly. The first principal direction is towards a direction of maximum variance of the data points, while the surface grows in more directions that automatically account for more variance of the data points.

4 Examples

This section contains a set of simulated data sets and two real data sets that illustrate the use of the principal sub-manifold.

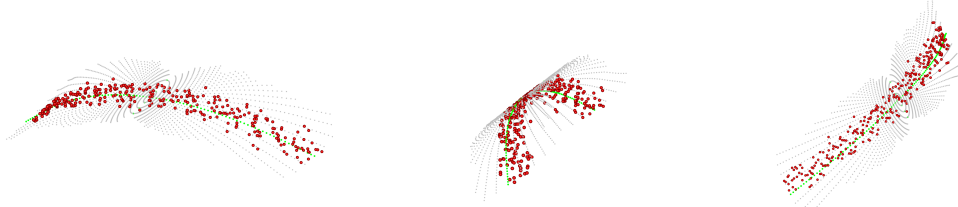


Figure 5: Visualization of the projected two-dimensional sub-manifold for data on S^3 , from three different view points. The data points are labeled in red, with the first and second principal direction (in green) going through the starting point. The sub-manifold (in gray) are constructed by Algorithm 1. For visualization purpose, the sub-manifold, the first and second principal direction and the data points have been projected to the first three eigenvectors of the covariance matrix at the starting point.

4.1 Simulated data

To further investigate the behavior of the principal sub-manifold as dependent on the configuration of the data points and the choice of scale parameter, we considered three sets of examples on S^3 . We chose this surface as a “test manifold” since it represents one of the most natural spaces from which the projected sub-manifold can be well understood, and since it provides a manifold for which we can compare the principal sub-manifolds with the principal geodesic. We observe here that the full manifold variation of the sub-manifold from the data can be very complicated; hence, we do not look at them on a quantitative basis, but rather investigate them qualitatively.

The first set of examples involves five data clouds in S^3 with each presenting a different curvature. As the curvature is non-constant, the Fréchet mean is no longer a good starting point for the principal sub-manifold. Instead, we choose the center of symmetry for each data as a starting point. The first and second data cloud are constructed in a way that the first three coordinates of each point are concentrated around a one dimensional curve; the configuration of the third and fourth are such that the points are on a two-dimensional surface/plane; the fifth one is much more diffuse: the points lie on a sea-wave-like surface.

For each one of them, a two-dimensional principal sub-manifold was fitted using three different h and the results are presented. The results indicate that the corresponding sub-manifolds perform well in capturing the local and global variation. We note that the sub-manifold fits well for data Cloud 1 no matter what scale of h is used (Figure 6(a)-(c)); the sub-manifold seems to capture a finer structure with a reduced value for h for data Cloud 2 (Figure 6(d)-(f)): this can be also seen as the first principal direction evolves with the scale of h . When the surface becomes two-dimensional for data Clouds 3 and 4, the principal sub-manifolds also excel: the fitted sub-manifold remains unchanged for different h as the surface is flat (Figure 6(g)-(i)), while it picks up the appropriate structure with a reduced h for bended surface (Figure 6(j)-(l)); For the cloud 5 (Figure 6(m)-(o)), it is more obvious that using a sub-manifold is more appealing than using only a curve or its equivalent; the sub-manifold fits the data points surprisingly well even with a surface of high curvature.

To probe how a sub-manifold performs with a noisy surface, we created four sets of data by blurring the sea-wave-like surface aforementioned with increasing levels of noise. Although the data reside in S^3 , most of the variation originates around a surface but not exactly on the surface. By knowing how the data points lie around the surface, we can get

a sense of such variability. As we should no longer look at the local scale when the points tend to have large variability, we found a two-dimensional sub-manifold by choosing an appropriate scale parameter h , potentially a larger one, for each data set. In Figure 7(a), when there is no noise, it is expected that the sub-manifold would capture total variation of the data in the projected space. When the noise increases (Figure 7(b) (c), and (d)), where all points are more diffused away from the underlying projected surface, the fitted sub-manifold is, although not a perfect sub-manifold, still well explaining for total data variability.

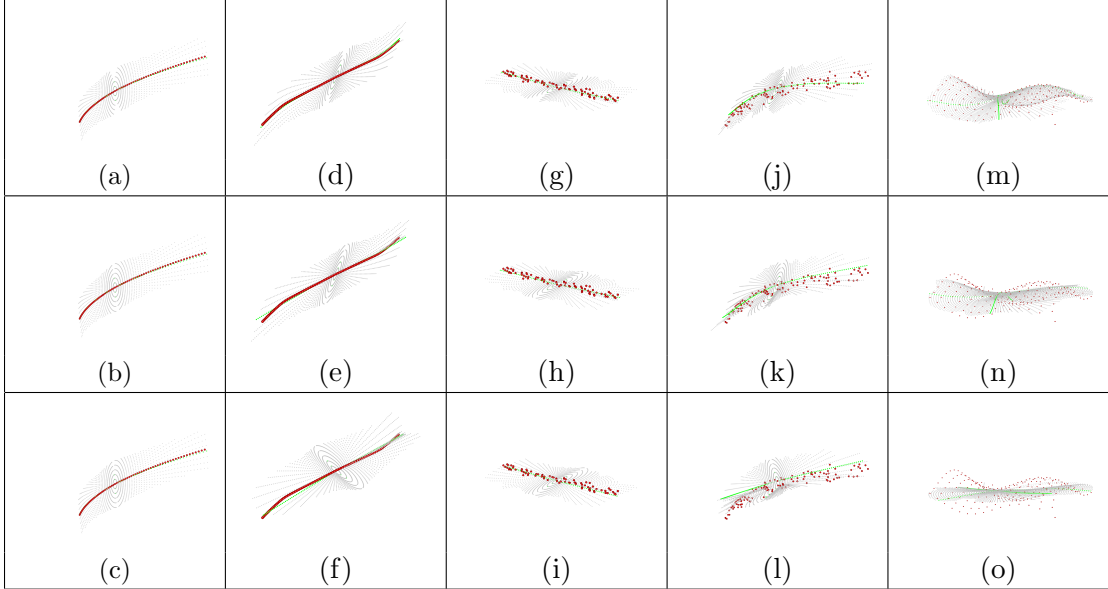


Figure 6: Principal sub-manifolds (with superimposed principal directions) for five data clouds in S^3 , with different scale parameters. (a)-(c) Principal sub-manifolds (in gray) and principal directions (in green) for data Cloud 1 (in red) for different values of h (small, middle, large). (d)-(f), (g)-(i), (j)-(l) and (m)-(o) provide the same information for data Clouds 2, 3, 4 and 5.

The last sets of examples are from a “lifted” ellipsoid in S^3 . Intuitively, the four data sets we generated represent different but inter-connected types of situation: (1) the triplets are well spread out inside the ellipsoid; (2)-(3) the triplets are mostly being concentrated in the middle of a more flatter ellipsoid; (4) the triplets are chosen nearly on the diameter of the ellipsoid (potentially around an ellipse). For case (1) (Figure 9(a)), where most points are inside the ellipsoid, neither one-dimensional nor two-dimensional sub-manifold would be a perfect sub-manifold. As the diffusion decreases, such as in case (2) (Figure 9(b)) and (3) (Figure 9(c)), the sub-manifold of dimension two appears to be more and more appropriate. In case (4) (Figure 9(d)), the sub-manifold provides the best fit such that all the projected data points lie on the sub-manifold. As one has already observed, the contribution of a two-dimensional sub-manifold in this example is only marginal. Arguably though, one can go further, for instance, having a higher dimensional sub-manifold in case (1) or case (2). Such extension of the algorithm would be very natural, but the details of implementing the algorithm are quite subtle and we choose not to proceed further.

To contrast the principal sub-manifold with the standard principal geodesic, we include the results of principal geodesics adjusted to its 2d version, for the case of Figure 6(j) and Figure 6(m). Specifically, the best h has been chosen for either method to perform

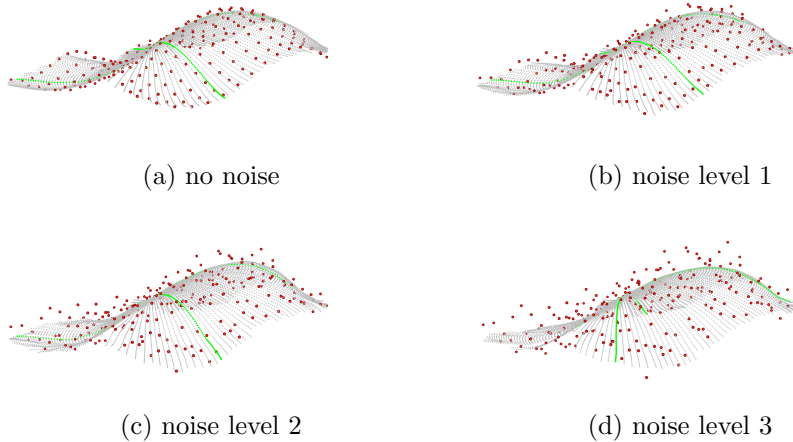


Figure 7: Principal sub-manifolds (with superimposed principal directions) for four sea wave sets of data with noise on S^3 . (a) Principal sub-manifolds with no noise added. (b), (c) and (d) provide the same information for three different levels of noise.

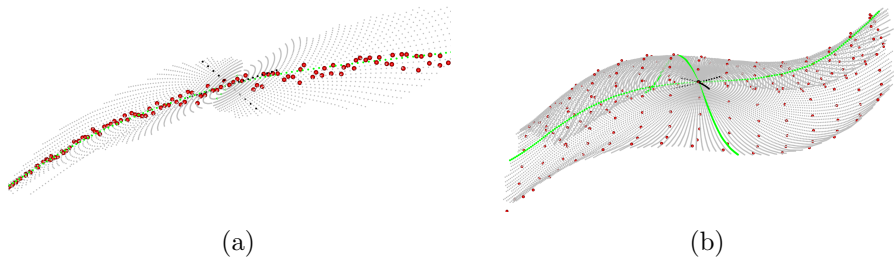


Figure 8: Comparison of principal sub-manifolds and principal geodesics. The principal geodesics (in black) are superimposed to the principal directions (in green) in the projected space. Only segments of the principal geodesics are highlighted for visualization purpose.

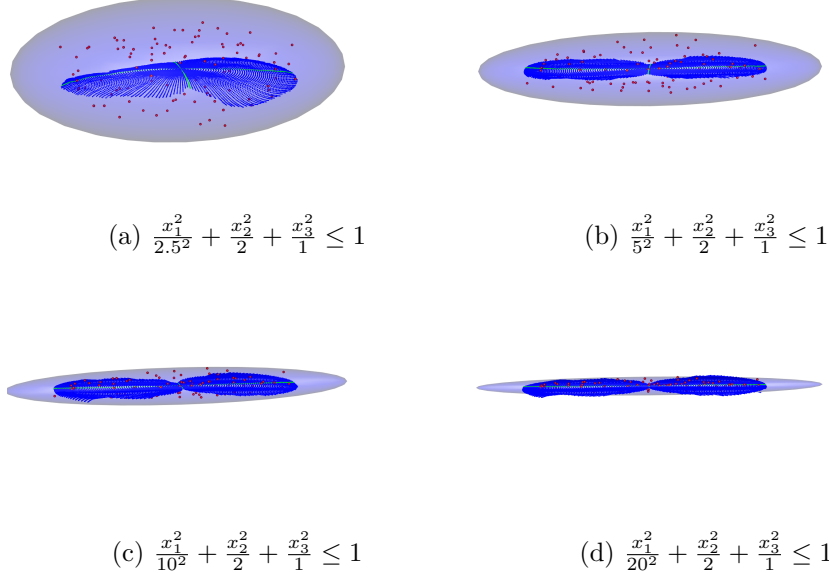


Figure 9: Principal sub-manifolds (with superimposed principal directions) for four ellipsoid sets of data on S^3 . (a) Principal sub-manifolds (in blue) and principal directions (in green) for data set (in red) of case (1). (b), (c) and (d) provide the same information for case (2), (3) and (4).

appropriately. It is expected that the principal geodesic, essentially a principal great circle along its first and second principal component, is not capable of capturing the curvature of the manifold; that is, the two principal geodesics (in black) for both cases (Figure 8(a)) and (Figure 8(b)) tend to deviate from the principal directions (in green) shortly after the starting point, thus not lying on the surface. In contrast, the principal sub-manifold handles the curvature well in both cases.

4.2 Principal variation of handwritten digits

To illustrate the use of the principal sub-manifold in a concrete example, we first consider a handwritten digit “3” data. The data consists of 13 landmarks of a “3” in two dimensions, collected from 30 individuals. For visualization, we find a principal sub-manifold for the data and recover the shape variation of the “3” in four principal directions, started at two different shapes of the “3”. In the first case (see Figure 11), the sub-manifold starts from the Fréchet mean of the data. In each principal direction, the flow of images describes the shapes of the ‘3’ moving from one extreme to the other extreme. The horizontal set of the images represents the various shapes of “3” recovered from the first principal direction. From there, we can see that the most varying part is the middle part of the “3.” The parts varying in the second principal direction are mainly the upper and lower parts of the “3.” Those parts of the “3” have exhibited a significant shape change along the two principal directions. Both the main diagonal and the other diagonal show certain degrees of the shape change mostly in the middle part of the “3” but in an opposite direction. By observing the fact that there are two seemingly outlying individuals of “3”s deviating from the rest in the data—the mean having moved away from the actual center of the data—a more sensible center of symmetry should be also considered. As in the second case (see Figure 2

of Supplementary Materials) serves to illustrate the slight effect of having a different choice (center of symmetry) of the starting point on the sub-manifold. However, no significant change in the representation of the sub-manifold is found.

To further understand the shape variation in configuration space, we contrast the results with that from the standard generalized Procrustes analysis (GPA). The profiling of shapes obtained from both methods along different principal directions (or principal components) in Figure 10 has suggested quite different patterns. Not only does the variation differ at various parts of the “3”, but the images of shapes recovered from the principal directions of the sub-manifold reveals asymmetrical variation around the Procrustes mean, compared to the GPA. This is expected as the curves along the principal directions of the sub-manifold vary in terms of their length, while the GPA profiles the images in the configuration space where it obeys a standard PCA manner.

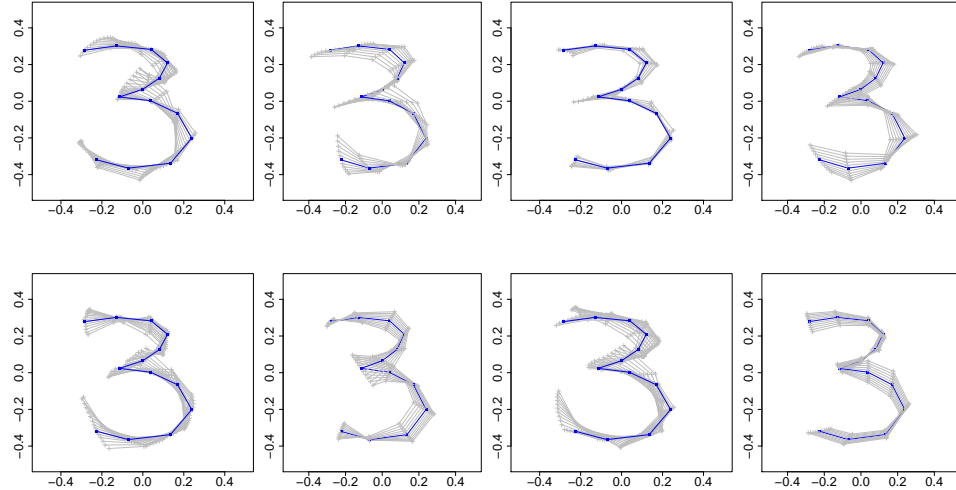


Figure 10: Principal sub-manifolds and generalized Procrustes analysis on the handwritten digits data. Upper left figures: the central figure (in blue) is the Procrustes mean; left figure contains images recovered from the first principal direction of the principal sub-manifold; right figure contains images recovered from the first principal component of generalized Procrustes analysis. Upper right, lower left, and lower right give the same information for second, third and fourth principal direction (or principal component) of the principal sub-manifold (or generalized Procrustes analysis).

4.3 Principal variation of leaf growth

We also considered a landmark data set consisting of leaf growth, collected from three Clones and a reference tree of young black Canadian poplars at an experimental site at the University of Göttingen. The landmark configurations of the leaves were collected from three Clones (‘C1’, ‘C2’, ‘C3’) and a reference tree (‘r’) collected at two different levels: breast height (Level 1) and the crown (Level 2). They consist of the shapes of 27 leaves (nine from Level 1 and eighteen from Level 2) from Clone 1; of 22 leaves (six from Level 1 and sixteen from Level 2) from Clone 2; and of 24 leaves (eighteen from Level 1 and seventeen from Level 2) from Clone 3 as well as of the shapes of 21 leaves (thirteen from Level 1 and eighteen from Level 2) from the reference tree, all of which

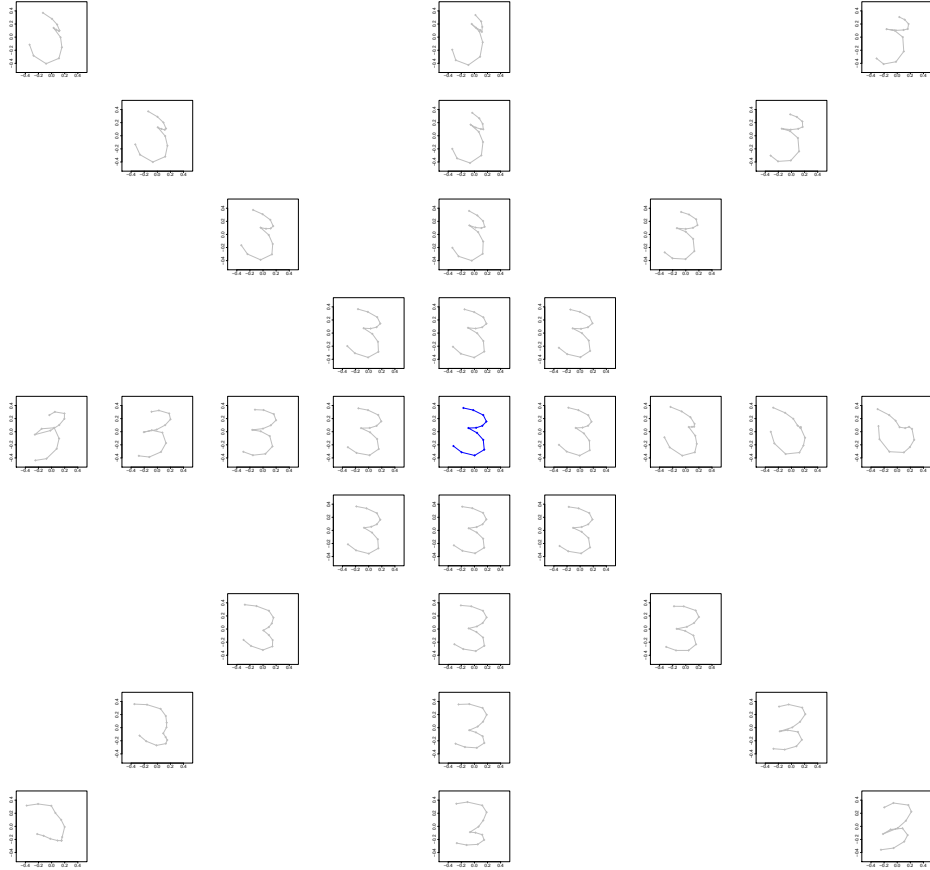


Figure 11: Principal sub-manifolds of the handwritten digits data, started from the mean. Among all the figures: the central figure (in blue) is the Fréchet mean; the horizontal row contains images recovered from the first principal direction of the sub-manifold; the vertical column is the second principal direction; the main diagonal is the third principal direction; the other diagonal is the fourth principal direction.

have been recorded non-destructively over several days during a major portion of their growing period of approximately one month. There are four landmarks corresponding to quadrangular configuration at petiole, tip, and largest extensions orthogonal to the connecting line. Figure 12 represents the four landmarks extracted from the contour image of each leaf on a flat plane, the four landmarks contain, in particular, the information of length, width, vertical and horizontal asymmetry.

Although it is known that the leaf growth of the genetically identical trees along a period of time reveals a non-Euclidean pattern [7], the study only focused on the mean geodesic difference (therefore essentially a one-dimensional variation), which is used for the discriminant analysis across the trees. However, the shape change along different directions—especially the principal directions in shape space—has not been fully explored. We will investigate the shape variation using principal sub-manifold among three Clones and the reference tree. As can be expected (see in Section 2.2), each landmark configuration, represented by a polygon in Figure 12, corresponds to a point in Kendall shape space. We focus on the non-geodesic shape variation primarily in vertical and horizontal direction of the leaf growth, the analysis of which requires a multi-dimensional scale treatment.

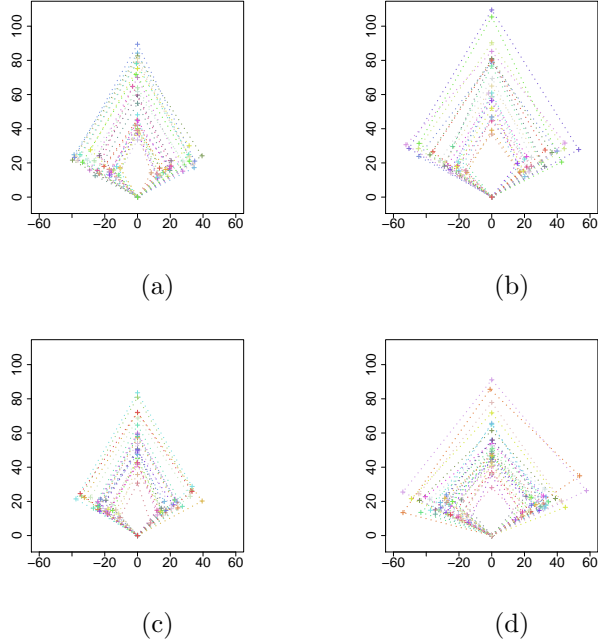


Figure 12: Leaf growth over a growing period of Clone 1 (a), Clone 2 (b), Clone 3 (c), and a reference tree (d). (a) Four landmarks on the leaf of Clone 1 have been connected and represented by a polygon at each growing period (27 polygons totally); (b)-(d) provide the same information for Clone 2 (22 polygons), Clone 3 (24 polygons) and the reference tree (31 polygons).

As all the leaves are very young, we first combine the leaves from the breast height and crown for each tree. For each tree, a principal sub-manifold is found, where two principal directions are extracted from the fitted sub-manifold. The two principal directions are then transformed to the preshape space and all the landmarks recovered are superimposed. Results for all the three Clones and the reference tree are displayed in Figure 13. The leaves of the reference tree exhibit two main kinds of variation: the first one tends to follow the horizontal direction with some effects along the vertical direction at tip. This can be well seen by the first principal direction in Figure 13(a); the second one concentrates on petiole, which is displayed by the second principal direction in Figure 13(b). The three Clones reveal different patterns of variation from the reference tree; between them, each differs from the other. Clone 1 shows more variation at the petiole and the left extension in the first principal direction, while the second principal direction shows more variation at the right extension; the two principal directions of Clone 2 behave more similarly as that of the reference tree, with some other variation appearing in the second principal direction of Clone 2 at the right extension and the tip; unlike Clone 1 and 2, variation in both vertical and horizontal directions appear evenly in either the first or the second principal direction for Clone 3. The same analysis for the leaves at breast height and crown alone has also been performed separately with a similar outcome, as shown in Figure 14, the result suggesting no different conclusion.

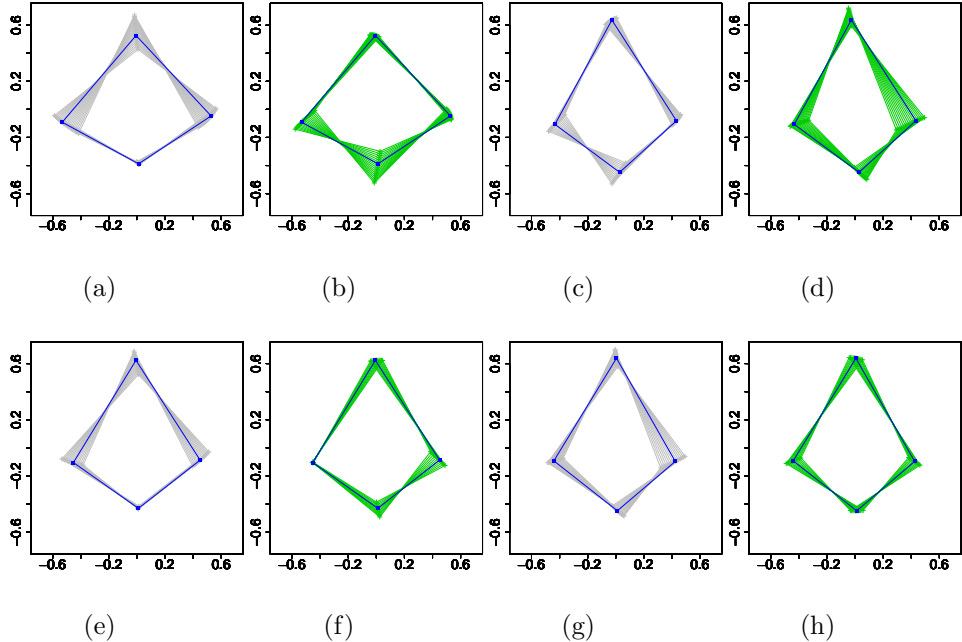


Figure 13: Principal sub-manifolds of the leaf growth data. (a) First principal direction obtained from the combined leaves at breast height and the crown of the reference tree; (b) Second principal direction obtained from the combined leaves at breast height and the crown of the reference tree. (c)-(h) provide the same information for Clone 1, 2 and 3.

5 Discussion

The statistical analysis of data on Riemannian manifold is a very challenging topic and it plays an increasingly important role in real-world problems. Conventional approaches, such as PCA in Euclidean space, are essentially helpful in neither learning the shape of the underlying manifold nor deciding its dimensionality. The main reason for this lies in the fact that those approaches simply do not use the intrinsic Riemannian manifold structures.

With the aim of proposing a method that allows for finding a nonlinear manifold from the data, we introduced the notation of principal sub-manifold. We showed the importance of estimating a multi-dimensional sub-manifold, and its difference from finding only a one-dimensional curve. The principal sub-manifold was seen to be interpretable as a measure of non-geodesic variation of the data. Based on a polar coordinate representation, the principal sub-manifold was constructed so that it coordinated with the local data variation. We illustrated that the principal sub-manifold is an extension of the principal flow, in the sense that it depicts a multi-dimensional manifold. When the manifold is linear, the principal sub-manifold reduces to the ball spanned by the usual principal components.

We claim here that by definition, the implemented principal directions might or might not coincide with the principal flows that are defined in [18], although in practice, they appear to be close to or the same as the principal flows. Under the polar coordinate representation, we observe that the principal directions (these are plotted in green in Figure 5) on the principal sub-manifold have presented the main modes of variation.

Regarding the issue of choosing the locality parameter h , or equivalently, at which scale of the local covariance should one consider? Admittedly, different sub-manifolds

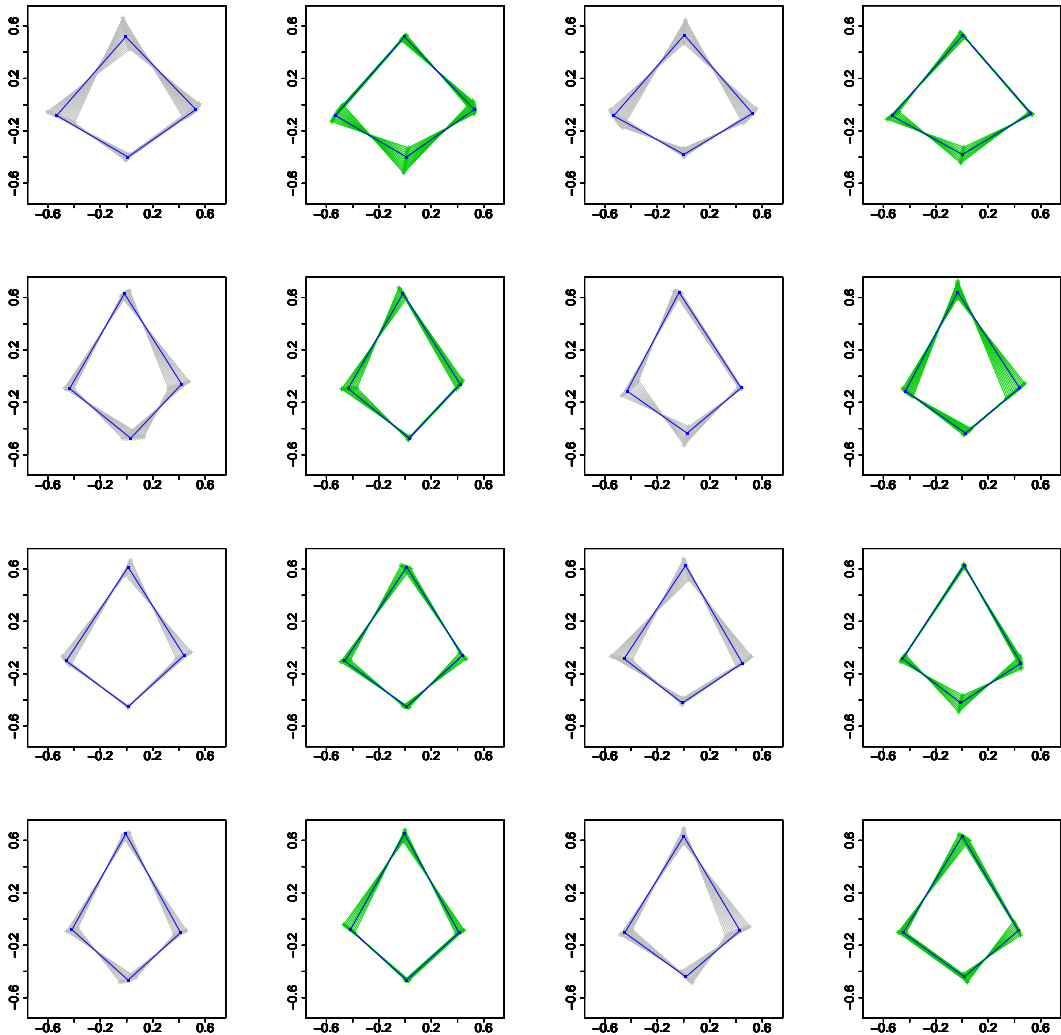


Figure 14: Principal sub-manifolds of the leaf growth data. Row 1 (reference tree): first principal direction at breast height; second principal direction at breast height; first principal direction at the crown; second principal direction at the crown. Row 2 - Row 4 provide the same information for Clone 1, 2 and 3.

would have been fitted by choosing different parameters. Still, we suggest not making a strict statement on optimizing the h ; rather, one should overview a sequence of h . We recommend the readers engage in a discussion of such choices associated with possible forms of criterion in [18] and the scale space perspective [1]. Simultaneously, we were able to define the principal sub-manifold to any dimension $k \leq d$, and this may also be seen as the development of a heuristic understanding of backward stepwise principle of PCA on manifolds: in the backward PCA, the best approximating affine subspaces are constructed from the highest dimension to the lowest one, see [11] for a spherical case of subspace, while in the case of principal sub-manifold, each net of the principal sub-manifolds (i.e., the principal directions) corresponds to the lower dimension sub-manifolds, compared to the entire sub-manifold.

Last but not least, the formulation of the principal sub-manifold opens the way to the generalization of many other statistical procedures. From the variance reduction perspective, one may think our proposed method as one of those competing methods that extend PCA on manifolds but not limited to only using lines or curves. This, potentially, can help us understand the data variation better and improve accuracy. From the classification point of view, this new method has been seen to be a useful tool to study shape changes. In the leaf growth example, we studied the only two main modes of shape variation. This has implied that one can extend a classification framework on the manifold. By projecting the new data points to any principal direction of the sub-manifold, one can calculate the distance and extend a classification rule based on all the distances. Surely, a successful classification also depends on 1) the data configuration; 2) how to define the local covariance matrix. If the data on the manifold is not too overlap, one might consider using a kernel density estimation. The label information needs also to be considered in the local covariance matrix, in which one would account for both of the between class and within class effects. As this is one of our on-going works, we will investigate it in the future.

Appendix A

Algorithm 1: two-dimensional principal sub-manifold

1. At a point A (mean or other point), use the logarithm map: $\log_A(x_i) = y_i$.
2. Find the covariance matrix $\Sigma_{A,\mathcal{M}}$ from y_1, \dots, y_n by (2.9).
3. Let $e_1(A)$ and $e_2(A)$ be the first and second eigenvector of $\Sigma_{A,\mathcal{M}}$. Define

$$Z_l = \epsilon' \times \left[\cos(2l\pi/L)e_1(A) + \sin(2l\pi/L)e_2(A) \right],$$

with $l = 1, \dots, L$.

4. Use exponential map to map Z_l onto \mathcal{M} so we get a set of new points $\exp_A(Z_l) = A_l$.
 5. Assume that we stay at point $A_{l,i}$, we are going to find $A_{l,i+1}$ ($A_{l,0} = A$ and $A_{l,1} = A_l$) via steps (a)-(g)
 - (a) find $\Sigma_{A_{l,i},\mathcal{M}}$.
 - (b) find $e_1(A_{l,i})$ and $e_2(A_{l,i})$.
 - (c) find $v_{l,i} = \log_{A_{l,i}}(A_{l,i-1})$.
 - (d) find

$$u_{l,i} = \langle v_{l,i}, e_1(A_{l,i}) \rangle e_1(A_{l,i}) + \langle v_{l,i}, e_2(A_{l,i}) \rangle e_2(A_{l,i})$$
 where $\langle a, b \rangle = \sum_{i=1}^n a_i b_i$ with $a = (a_1, \dots, a_n)$ and $b = (b_1, \dots, b_n)$.
 - (e) calculate

$$r_{l,i} = -\epsilon' \times \frac{u_{l,i}}{\|u_{l,i}\|}.$$
 - (f) update

$$A_{l,i+1} = \exp_{A_{l,i}}(r_{l,i}).$$
 - (g) stop at $A_{l,i+1}$ when

$$\|\log_{A_{l,i+1}}(x_j)\| > \delta \text{ or } \langle \log_{A_{l,i+1}}(A_{l,i}), \log_{A_{l,i+1}}(x_j) \rangle \geq 0.$$
 for all $j = 1, \dots, n$.
 6. For every $l = 1, \dots, L$, connect $A_{l,i}$ with $A_{l,i+1}$ by i we get \mathcal{A}_l , a net of principal sub-manifold.
 7. **Output:** all \mathcal{A}_l 's as in (3.12), where $1 \leq l \leq L$.
-

Remark: In Step 3, there is no difference in either forming a circle or an ellipse for small ϵ' . In case of an ellipse, the axes of ellipse would be proportional to the first and second eigenvalue of $\Sigma_{A,\mathcal{M}}$. In case of a k -dimensional sub-manifold, Step 3 and Step 5(b) will need to be updated with the first k eigenvectors.

Appendix B: Proof of Theorem 1

In the linear space \mathbb{R}^d ,

$$\Sigma_{B,\mathcal{M}} = \frac{1}{n} \sum_{i=1}^n (X_i - A)^\top (X_i - A) + (B - A)^\top (B - A).$$

By eigenvalue inequality,

$$\begin{aligned} \sum_{j=1}^k \lambda_j(B, \mathcal{M}) &\leq \sum_{j=1}^k \lambda_j(A, \mathcal{M}) + \text{trace}\left((B - A)^\top (B - A)\right) = \sum_{j=1}^k \lambda_j(A, \mathcal{M}) \\ &\quad + \|B - A\|^2. \end{aligned}$$

Let $D = \log_A(B)$, then

$$\|B - A\|^2 \leq \|D - A\|^2.$$

Putting all the results together,

$$\begin{aligned} \int_{D \in \log_A(\mathcal{N})} \left(\cos(\alpha_B) \times \sum_{j=1}^k \lambda_j(B, \mathcal{M}) \right) d\mu_k &\leq \int_{D \in \log_A(\mathcal{N})} \left(\sum_{j=1}^k \lambda_j(B, \mathcal{M}) \right) d\mu_k \\ &\leq \int_{D \in \log_A(\mathcal{N})} \left(\sum_{j=1}^k \lambda_j(A, \mathcal{M}) + \|D - A\|^2 \right) d\mu_k \\ &= \int_{D \in \log_A(\mathcal{N})} \sum_{j=1}^k \lambda_j(D, \log_A(\mathcal{N})) d\mu_k. \end{aligned}$$

The inequality becomes equality when \mathcal{N} is a linear space spanned by $e_1(A, \mathcal{M}), e_2(A, \mathcal{M}), \dots, e_k(A, \mathcal{M})$.

References

- [1] Probal Chaudhuri and J. S. Marron. Scale space view of curve estimation. *The Annals of Statistics*, 28:408–428, 2000.
- [2] R. Fisher. Dispersion on a sphere. *Proceedings of the Royal Society A: Mathematical, Physical and Engineering Science*, 217:295–305, 1953.
- [3] P. T. Fletcher and S. Joshi. Riemannian geometry for the statistical analysis of diffusion tensor data. *Signal Processing*, 87:250–262, 2007.
- [4] P. T. Fletcher, C. Lu, S. M. Pizer, and S. Joshi. Principal geodesic analysis for the study of nonlinear statistics of shape. *IEEE Transactions on Medical Imaging*, 23:995–1005, 2004.
- [5] S. Gerber, T. Tasdizen, P. T. Fletcher, S. Joshi, R. Whitaker, and the Alzheimers Disease Neuroimaging Initiative (ADNI). Manifold modeling for brain population analysis. *Medical Image Analysis*, 14:643–653, 2010.
- [6] T. Hastie and W. Stuetzle. Principal curves. *Journal of the American Statistical Association*, 84:502–516, 1989.

- [7] S. Huckemann. Intrinsic inference on the mean geodesic of planar shapes and tree discrimination by leaf growth. *The Annals of Statistics*, 39:1098–1124, 2011.
- [8] S. Huckemann, T. Hotz, and A. Munk. Intrinsic shape analysis: Geodesic pca for riemannian manifolds modulo isometric lie group actions. *Statistica Sinica*, 20:1–100, 2010.
- [9] S. Huckemann and H. Ziezold. Principal component analysis for riemannian manifolds, with an application to triangular shape spaces. *Advances in Applied Probability*, 38:299–319, 2006.
- [10] S. Jung, I. L. Dryden, and J. S. Marron. Analysis of principal nested spheres. *Biometrika*, 99:551–568, 2012.
- [11] S. Jung, X. Liu, J. S. Marron, and S. M. Pizer. *Generalized PCA via the backward stepwise approach in image analysis*, volume 83, pages 111–123. 2010.
- [12] P. E. Jupp and J. T. Kent. Fitting smooth paths to spherical data. *Journal of the Royal Statistical Society, Series C*, 36:34–36, 1987.
- [13] H. Karcher. Riemannian center of mass and mollifier smoothing. *Communication on Pure and Applied Mathematics*, 30:509–541, 1977.
- [14] D. G. Kendall. A survey of the statistical theory of shape. *Statistical Science*, 4(2):87–120, 1989.
- [15] D. G. Kendall, D. Barden, T. K. Carne, and H. Le. *Shape and Shape Theory*. Wiley, New York, 1999.
- [16] K. Kenobi, I. L. Dryden, and H. Le. “shape curves and geodesic modelling. *Biometrika*, 97:567–584, 2010.
- [17] A. Kume, I. L. Dryden, and H. Le. Shape-space smoothing splines for planar landmark data. *Biometrika*, 94:513–528, 2007.
- [18] V. M. Panaretos, T. Pham, and Z. Yao. Principal flows. *Journal of the American Statistical Association*, 109:424–436, 2014.
- [19] X. Pennec. Intrinsic statistics on riemannian manifolds: Basic tools for geometric measurements. *Journal of Mathematical Imaging and Vision*, 25:127–154, 2006.
- [20] X. Pennec. Barycentric subspaces and affine spans in manifolds. In *Geometric Science of Information (GSI) 2015*, pages 12–21. Springer International Publishing, 2015.
- [21] X. Pennec and J.-P. Thirion. A framework for uncertainty and validation of 3d registration a framework for uncertainty and validation of 3d registration methods based on points and frames. *Int. Journal of Computer Vision*, 25:203–229, 1997.
- [22] S. Sommer. Horizontal dimensionality reduction and iterated frame bundle development. In *Geometric Science of Information (GSI) 2013*, pages 76–83. Springer: Berlin/Heidelberg, 2013.
- [23] R. Souvenir and R. Pless. Image distance functions for manifold learning. *Image and Vision Computing*, 25(3):365–373, 2007.

- [24] Z. Zhang and H. Zha. Principal manifolds and nonlinear dimensionality reduction via tangent space alignment. *SIAM journal on scientific computing*, 26(1):313–338, 2004.